Prediction of quantum interference in molecular junctions using a parabolic diagram: Understanding the origin of Fano and anti- resonances

2013 J. Phys.: Conf. Ser. 427 012013

(http://iopscience.iop.org/1742-6596/427/1/012013)

Journal of Physics: Conference Series **427** (2013) 012013 doi:10.1088/1742-6596/427/1/012013

Prediction of quantum interference in molecular junctions using a parabolic diagram: Understanding the origin of Fano and anti- resonances

Daijiro Nozaki[1]*, Stanislav M. Avdoshenko[1,2], Hâldun Sevinçli[1,3], Rafael Gutierrez[1], and Gianaurelio Cuniberti[1,4]

[1] Institute for Materials Science and Max Bergmann Center of Biomaterials, Dresden University of Technology, 01062 Dresden, Germany
[2] School of Materials Engineering, Purdue University, West Lafayette, IN 47907-2045, USA
[3] Department of Micro- and Nanotechnology, Technical University of Denmark, Kongens Lyngby, Denmark
[4] Division of IT Convergence Engineering and National Center for Nanomaterials Technology, POSTECH, Pohang 790-784, Republic of Korea

E-mail: daijiro.nozaki@gmail.com

Abstract. Recently the interest in quantum interference (QI) phenomena in molecular devices (molecular junctions) has been growing due to the unique features observed in the transmission spectra. In order to design single molecular devices exploiting QI effects as desired, it is necessary to provide simple rules for predicting the appearance of QI effects such as anti-resonances or Fano line shapes and for controlling them. In this study, we derive a transmission function of a generic molecular junction with a side group (T-shaped molecular junction) using a minimal toy model. We developed a simple method to predict the appearance of quantum interference, Fano resonances or anti- resonances, and its position in the conductance spectrum by introducing a simple graphical representation (parabolic model). Using it we can easily visualize the relation between the key electronic parameters and the positions of normal resonant peaks and anti-resonant peaks induced by quantum interference in the conductance spectrum. We also demonstrate Fano and anti-resonance in T-shaped molecular junctions using a simple tight-binding model. This parabolic model enables one to infer on-site energies of T-shaped molecules and the coupling between side group and main conduction channel from transmission spectra.

1. Introduction

Quantum interference (QI) effects, which are interference phenomena between waves observed in nanostructures, in *electron transport* systems have been broadly studied in the field of mesoscopic physics and quantum dots [1, 2, 3] and their appearance in molecular junctions had been proposed in the early 1990s from studies of electron transfer [4, 5, 6]. Recently QI effects in electron transport through molecular wires have increasingly gained interest due to the unique spectral features observed in conductance spectra [7, 8, 9, 10, 11, 12, 13, 14, 15]. This is not only of great interest from a fundamental point of view, but also from a practical one. Since QI effect can dramatically change the electron transmission at low energies (around the Fermi energy), it can be used for many applications such as molecular switches [14], sensors, and interferometers, and

thermoelectric devices [16]. For instance, QI spectral features emerging around the Fermi energy may lead to dramatic changes in the Seebeck coefficient of a molecular junction and thus make it a relevant candidate for molecular scale thermoelectric applications [16]. Therefore, in order to tune QI related spectral features, it is crucial to be able to develop a basic understanding of the conditions under which QI effects appear as well as their dependence on the molecular electronic structure. Although this can be achieved via time-consuming first-principle calculations in each specific case, it is desirable (also for the experimentalists working in the field of nanoscale electronics) to provide simple yet accurate rules able to predict the emergence and type of QI based structures in molecular junctions.

In this report, we are able to give a rather simple answer to some fundamental questions: Why does quantum interference appear in certain molecules? Which particular features have T-shaped molecular junctions, which manifest in the existence of both Fano-type and antiresonance line shapes? What is the relationship between QI effects and the low energy electronic structure of the molecular systems [17]? To address these problems, we deal with a toy model of a T-shaped molecular junction and introduce a simple yet accurate graphical representation (which we called the parabolic diagram for the sake of simplicity) that allows for a clear visualization of the relationship between different key electronic structure parameters of the molecule and the existence of different QI related features in the conductance spectrum (Fano resonances and anti-resonances). Using this simple approach, we can predict which type of QI effect can be expected in T-shaped junctions according to the specific electronic structure of the molecular system.

This report is organized as follows. In the next section, we derive the transmission function of generic molecular junctions with a side functional group using a toy model, and introduce a parabolic model that we developed. In section 3, we test the parabolic model and demonstrate two types of QI-related line shapes (anti-resonance and Fano resonance) in a simple two site approximation. In section 4, we demonstrate Fano and anti-resonance in T-shaped molecular junctions using the Hückel model. We conclude this report in section 5.

2. Parabolic model

In this section, we derive an expression for the transmission functions of T-junctions made from molecular wires with side functional groups. The derivation is also given in [16, 8] in a similar way. Then we introduce a parabolic diagram to predict the position of QI-effect in the transmission spectra. This parabolic model enables one to visualize the relationship between electronic parameters and the positions of negative and positive peaks in the transmission spectra.

For simplicity, we consider a T-shaped molecule consisting of two sites coupled between two contacts as shown in Fig. 1. The molecule is attached to left and right contacts only through the central site, i.e. the side group do not directly couple to the contacts. Hamiltonian matrix and overlap matrix for the molecule are given by:

$$H_M = \begin{bmatrix} \varepsilon_0 & V \\ V & \varepsilon_1 \end{bmatrix}, S_M = \begin{bmatrix} 1 & S \\ S & 1 \end{bmatrix}. \tag{1}$$

The on-site energies for the central site and the side group are given by ε_0 and ε_1, respectively. Those are coupled by V. The retarded Green's function $G^r(E)$ for this system in orthogonal basis is given by

$$[G^r(E)] \begin{bmatrix} E + i\delta - \varepsilon_0 - \Sigma_{\mathrm{L}}(E) - \Sigma_{\mathrm{R}}(E) & -V \\ -V & E + i\delta - \varepsilon_1 \end{bmatrix} = \begin{bmatrix} 1 & 0 \\ 0 & 1 \end{bmatrix}, \tag{2}$$

where $\Sigma_{\mathrm{L/R}}(E) = \eta(E) + i\gamma(E) = \mathrm{Re}[\Sigma_{\mathrm{L/R}}(E)] + i\mathrm{Im}[\Sigma_{\mathrm{L/R}}(E)]$ are self-energy terms for left/right contacts and $i\delta$ is infinitesimal imaginary value. Equation (2) can be written in scalar value as:

$$G^r(E) = (E + i\delta) - \varepsilon_0 - \Sigma_{\rm L}(E) - \Sigma_{\rm R}(E) - \frac{V^2}{E - \varepsilon_1} \tag{3}$$

Using the Fisher-Lee relation [18], the transmission function $T(E)$ is given by

$$T(E) \equiv {\rm Tr}[\Gamma_{\rm L}(E)G^r(E)\Gamma_{\rm R}(E)G^a(E)] = \frac{4\gamma(E)^2}{(E - \varepsilon_0 - 2\eta(E) - \frac{V^2}{E-\varepsilon_1})^2 + 4\gamma(E)^2}, \tag{4}$$

where $\Gamma_{\rm L/R}(E)$ are the broadening functions defined as $\Gamma_{\rm L/R}(E) \equiv i[\Sigma_{\rm L/R} - \Sigma^\dagger_{\rm L/R}]$. If we apply the wide band limit (WBL), $\Sigma_{\rm L/R}(E) = -i\gamma$, with no energy dependence to $\gamma(E)$. The transmission function is given by

$$T(E) = \frac{4\gamma^2}{(E - \varepsilon_0 - \frac{V^2}{E-\varepsilon_1})^2 + 4\gamma^2}. \tag{5}$$

This transmission function $T(E)$ has Breit-Wigner-type resonances [19] showing the maxima ($T(E) = 1$) with broadening γ at the energies where the term in the denominator in eq. (5) satisfies $(E - \varepsilon_0 - \frac{V^2}{E-\varepsilon_1}) = 0$. These peaks correspond to eigen-states of the molecular system and two solutions of $(E - \varepsilon_0 - \frac{V^2}{E-\varepsilon_1}) = 0$ are given by

$$\varepsilon_{\rm VB,CB} = \frac{\varepsilon_0 + \varepsilon_1 \pm \sqrt{(\varepsilon_0 - \varepsilon_1)^2 + 4V^2}}{2}. \tag{6}$$

Interestingly, $T(E)$ shows a QI-induced negative peak (antiresonance) with a minimum ($T(E) = 0$) at $E = \varepsilon_1$ since the denominator in eq. (4) diverges at $E = \varepsilon_1$.

Here we introduce a parabolic diagram to visualize the relationship between electronic parameters (ε_0, ε_1, V) and the energetic positions of Breit-Wigner-type resonances ($E = \varepsilon_{\rm VB}, \varepsilon_{\rm CB}$) and the QI-induced anti-resonance ($E = \varepsilon_0$) in the transmission spectra [17]. The position of the two Breit-Wigner-type resonances can be easily estimated by depicting the parabolic curve, $y = (E - \varepsilon_1)(E - \varepsilon_0)$, as shown in Fig. 1(b). The two intersection points between the line $y = V^2$ and the parabolic curve are the energetic positions of Breit-Wigner-type resonances ($E = \varepsilon_{\rm VB,CB}$) since eq. (5) at $E = \varepsilon_{\rm VB,CB}$ gives $T(E) = 1$. As for the energetic position of the antiresonance in the transmission spectra, it is obvious that $E = \varepsilon_1$ gives a negative peak ($T(E) = 0$) from eq. (5) because of the divergence of denominator at $E = \varepsilon_1$.

This is how we can easily visualize the position of Breit-Wigner-type positive peaks and the QI-induced negative peak in transmission spectra from the parabolic model in Fig. 1(b). Figure 1(c) shows the transmission spectra of the T-shaped molecular junction in Fig. 1(a) from eq. (5) using the same parameters in Fig. 1(b); $\varepsilon_0 = 0.0$ eV, $\varepsilon_1 = 3.0$ eV, $V^2 = 2.0$ eV^2, and $\gamma = 0.01$. We can see that the position of the negative and positive peaks completely matches with the features of the parabolic diagram. The merit of the parabolic model is that if we observe the Breit-Wigner-type resonances and the anti-resonance in conductance spectra by measurement, it is possible to determine the energies of the conduction channels and the localized states at the side group and their coupling from the parabolic diagram. Even in the non-WBL approximation, this parabolic model is valid as long as the energy-dependence of $\eta(E)$ in (4) is small, since the $\eta(E)$ in (4) just shifts the position of ε_0 in the quadratic equation $y = (E - \varepsilon_0)(E - \varepsilon_1)$ to ε_0', where $\varepsilon_0' = \varepsilon_0 + \eta(E)$. Although the inclusion of the $\eta(E)$ shifts the one of Breit-Wigner resonances at $E = \varepsilon_{\rm VB}$, this does not affect the energetic position of QI-induced anti-resonance at $E = \varepsilon_1$.

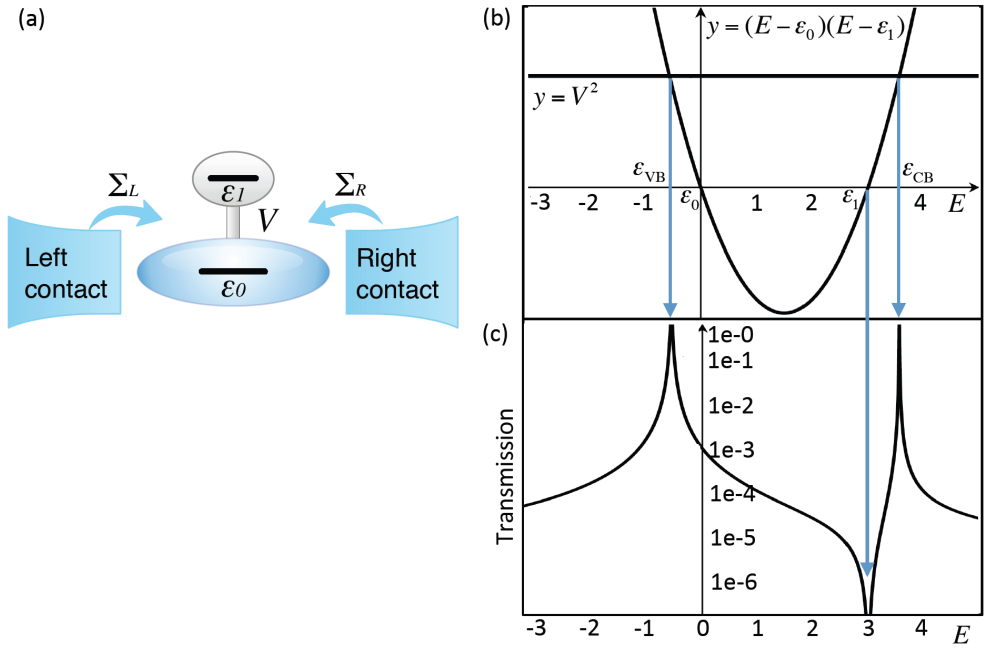

Figure 1: (a) Schematic image of a molecular junction with a side group considered in this work. A molecule consisting of two fragments is coupled between contacts. The energies of the two fragment molecular orbitals (MOs) are ε_0 and ε_1. The transfer integral between them is give by V. $\Sigma_{\mathrm{L/R}}$ represents the self-energies due to coupling to the contacts. (b) Parabolic diagram describing the relation between electronic parameters in (a). (c) Transmission spectrum through the molecular device depicted schematically on panel (a). The quantum interference appears as a abrupt negative peak in transmission spectrum and its position can be predicted from the parabolic model in panel (b). Parameters in (b) and (c) are set to $\varepsilon_0 = 0.0$ eV, $\varepsilon_1 = 3.0$ eV, $V^2 = 2.0$ eV^2, and $\gamma = 0.01$ eV.

3. Demonstration of Anti- and Fano resonances from the parabolic model

Our parabolic model is general and thus can be applied to any systems having T-shaped topology as shown in eq. (1) or Fig. 1(a). The results obtained in the simple model were further validated using first-principle quantum transport methods in realistic T-shaped molecular junctions. The expansion to the realistic molecular junctions including more than 2 sites are shown elsewhere (see Ref. [17]). In this section we demonstrate two types of interference patterns, anti- and Fano resonances, in transmission spectra using the parabolic model. The condition necessary to realize Fano resonance is to have large $|\varepsilon_1 - \varepsilon_0|/|V|$, while the condition necessary to realize anti-resonance is to have small $|\varepsilon_1 - \varepsilon_0|/|V|$. Figure 2 presents the transmission functions of the T-shaped molecular junction shown in Fig. 1(a) with difference coupling strengths, V. When the coupling V is reduced, one of the Breit-Wigner resonances and the QI-induced anti-resonance come close to each other forming a Fano resonance. This behavior can be easily understood from the parabolic diagram in Fig. 2(a).

Next, we examine how the energy difference between two on-site energies, $\varepsilon_1 - \varepsilon_0$, affects the quantum interference in transmission spectra. Figure 3 presents the transmission functions of the T-shaped molecular junctions in Fig. 1(a) with different on-site energies, ε_1. It is notable that when the sign of the term, $\varepsilon_0 - \varepsilon_1$, is changed from negative to positive, the phase of the Fano resonances is flipped for π. This feature enables one to know whether the energy of the state from side group, ε_1, is higher than the conducting state, ε_0. These trends can be also interpreted from the parabolic model as shown in Fig. 3(a).

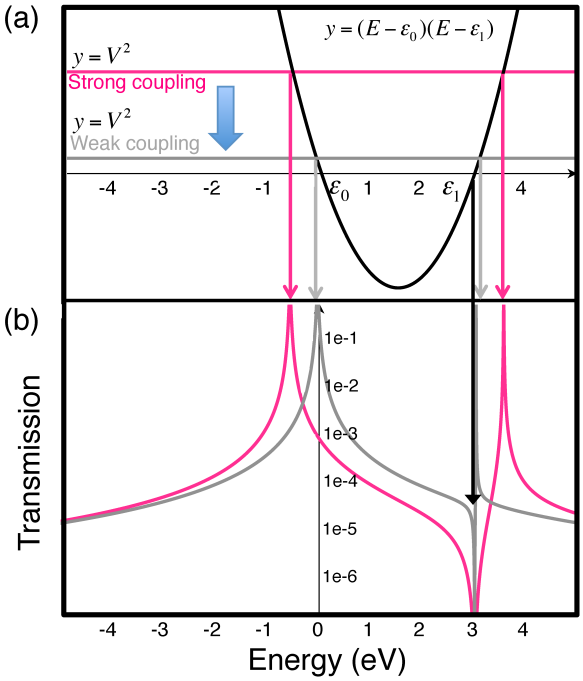

Figure 2: Coupling dependence of transmission functions in T-shaped molecular junctions in Fig. 1(a). Electronic parameters are set to $\varepsilon_0 = 0.0$ eV, $\varepsilon_1 = 3.0$ eV, $V^2 = 2.0$ eV^2 (strong coupling), $V^2 = 0.3$ eV^2 (weak coupling), and $\gamma = 0.01$ eV. (a) Parabolic diagram and (b) transmission spectrum through the molecular device depicted in Fig. 1(a). The quantum interference patterns gradually shift from anti-resonance to Fano resonance as the coupling V is reduced.

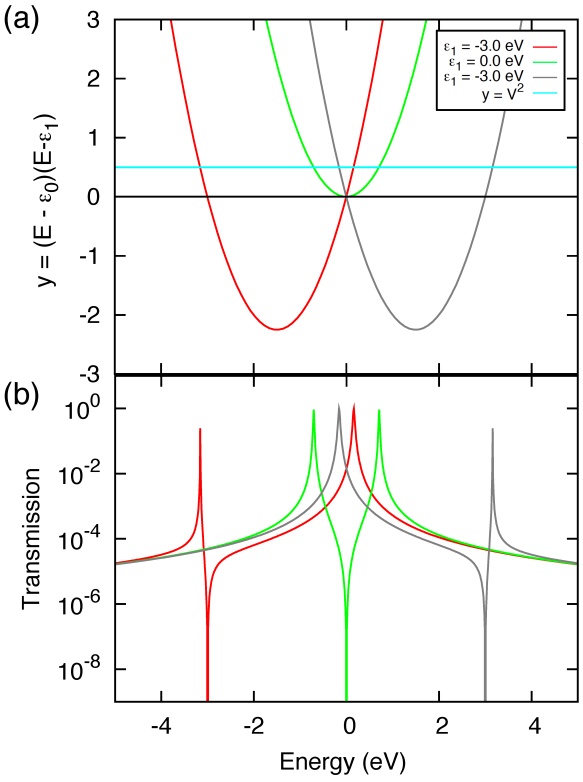

Figure 3: On-site energy dependence of transmission functions in T-shaped molecular junctions in Fig. 1(a). Electronic parameters are set to $\varepsilon_0 = 0.0$ eV, $V^2 = 0.5$ eV^2, and $\gamma = 0.01$ eV. The parameters for ε_1 are shown in the inset of (a). (a) Parabolic diagram and (b) transmission spectra through the molecular device depicted in Fig. 1(a) with different on-site energies for the side groups, ε_1. Depending on the sign of the term, $\varepsilon_0 - \varepsilon_1$, the phase of the Fano resonances is flipped for π.

Finally we investigate the density of states (DOS) of the T-shaped molecular devices. Fig. 4 shows the total DOS (TDOS) and projected DOS (PDOS) of the molecular system shown in Fig.1(a). The TDOS and two PDOS at $E = 0.0$ eV presents a normal Lorenzian-type resonance, while the PDOS plot of the conducting channel originating from the ε_0 state shows Fano resonance at $E = -3.0$ eV. We can see that the PDOS from the side group contributes to

almost all of the TDOS of the resonant peak at $E = -3.0$ eV. Therefore the state ε_1, which is weakly coupled to main conduction channel ε_0, is localized at the side group and can disturb the electron transport through the main conducting state ε_0 yielding a Fano resonance in transmission spectra. This behavior shows a good agreement with the well-known interpretation of the Fano resonance where a localized state interferes with the continuous state.

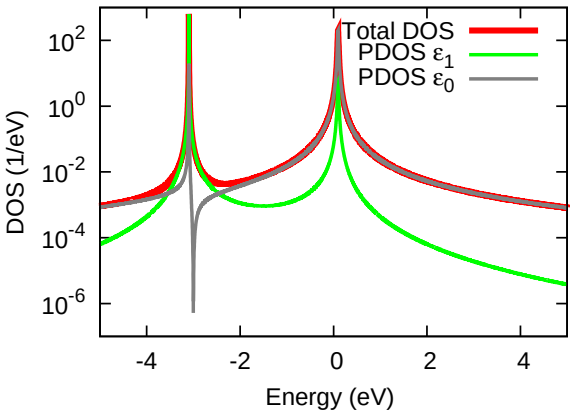

Figure 4: Density of states (DOS) in T-shaped molecular junctions in Fig. 1(a). Electronic parameters are set to $\varepsilon_0 = 0.0$ eV, $\varepsilon_1 = -3.0$ eV, $V^2 = 0.5$ eV^2, and $\gamma = 0.01$ eV. The peak at $E = -3.0$ eV in the TDOS plot originates from the localized state of the side group. Note that the projected DOS (PDOS) from the site ε_1 at $E = -3.0$ eV is much larger than the PDOS from the main conducting channel, ε_0. Because of the localized state from the side group, the conducting state in gray curve is subject to interference showing the Fano resonance at $E = -3.0$ eV.

4. Application of a parabolic model to molecular systems

Here we aim to demonstrate Fano and anti- resonances in the π-electron systems using a simple Hückel model. We modeled two T-shaped molecules named as model A and model B shown in Figs. 5 and Fig. 6 to realize Fano and anti- resonance, respectively. The condition to realize a Fano resonance in the transmission spectra is that the energy difference between the eigen energy of side fragment (ε_1) and that of main chain (ε_0) is large compared with the coupling V. This can be restated as the condition to realize a Fano resonance is that molecular junctions have localized local DOS (LDOS) at the side groups and those energies are separated enough from the energies of conducting states. On the other hand, if the energy difference $|\varepsilon_1 - \varepsilon_0|$) is small compared with the coupling V, molecular junctions will show an anti-resonance. Especially when an eigen energy of a side fragment is identical to that of the main chain, an anti-resonance will appear as we will see later.

In model A, pyrene is covalently attached to the main chain as a side group. The side group has HOMO and LUMO at $E = \pm 0.402\beta$, while the main chain has HOMO and LOMO at $E = \pm 0.215\beta$. The eigen energies of the side group are energetically separated from the ones of the main chain. The model A has large LDOS localized at the side group around $E = \pm 0.402\beta$ as shown in Fig. 5(d). Thus, model A satisfies the conditions for Fano resonances. Indeed, Fano resonances can be seen at $E = \pm 0.402\beta$ in Fig. 5(c). When the transfer integral V between the side group and the main chain is reduced, the Fano resonance gets sharper (see Fig. 7(a)).

In model B, the side group has almost same structure with the main chain. Thus, the eigen-energies of the side fragment are almost identical with that of the main chain. Thus, the resonant peaks of the main chain (pristine chain in 6(c)) in the transmission function split into two resonances after the attachment of the side group, showing an anti-resonance in the middle

of them. In these levels, molecular orbitals delocalize because of the orbital hybridization. This delocalization can be seen in the LDOS plots in Fig. 6(d). When the coupling with the side group is enhanced the resonant levels split further (see Fig. 7(b)). These features show a good agreement with parabolic analysis discussed in the previous section (see Figs. 2 and 3).

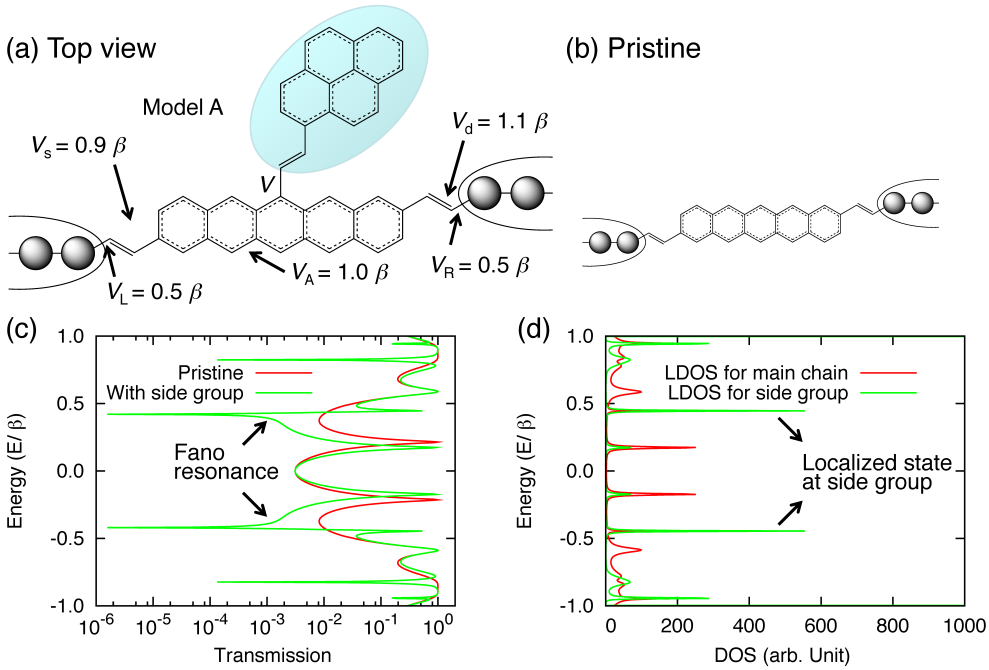

Figure 5: Demonstration of Fano resonance in a T-shaped molecular junction using the Hückel model: (a) Tight-binding scheme for a molecular junction (model A) with a side group using the Hückel model. Coupling between the molecule and left (right) 1D electrode is set to $V_{\mathrm{L/R}} = 0.5\beta$. The transfer integrals for aromatic carbons, single bond, and double bonds are set to $V_{\mathrm{A}} = 1.0\beta$, $V_{\mathrm{s}} = 0.9\beta$, and $V_{\mathrm{d}} = 1.1\beta$, respectively. The transfer integral V between the side chain and the main chain is set to $V = 0.9\beta$. All transfer integrals are normalized in β. Transfer integrals in the electrodes are set to β. All on-site energies are set to 0. Side group is highlighted in light blue. (b) Pristine molecular wire connected between two electrode for the comparison with the T-shaped molecular wires. (c) Transmission spectra through the molecular device depicted schematically on panel (a) and (b). Since the side fragment has eigenstates at $E = \pm 0.402\beta$ and these states localize at side group (see LDOS plot in (d)), Fano resonances appear at these energies. (d) local DOS plots for the side group and the main chain.

5. Conclusion

In order to understand the origin of quantum interference phenomena in electron transport systems with single side groups we have developed a simple but accurate toy model to predict the appearance and the positions of the quantum interference in transmission spectra. Introducing a parabolic diagram, the relationship between key electronic parameters and the line shape of the transmission spectra can be visualized. We have demonstrated two types of quantum interference phenomena namely, Fano and anti- resonances, in transmission spectra using the parabolic model. If observable peaks and dips of the conductance can be resolved experimentally, the conditions for quantum interference effects to appear can be visualized, thus the parabolic model potentially allows for tailoring the molecular system presenting Fano- or anti-resonance as desired.

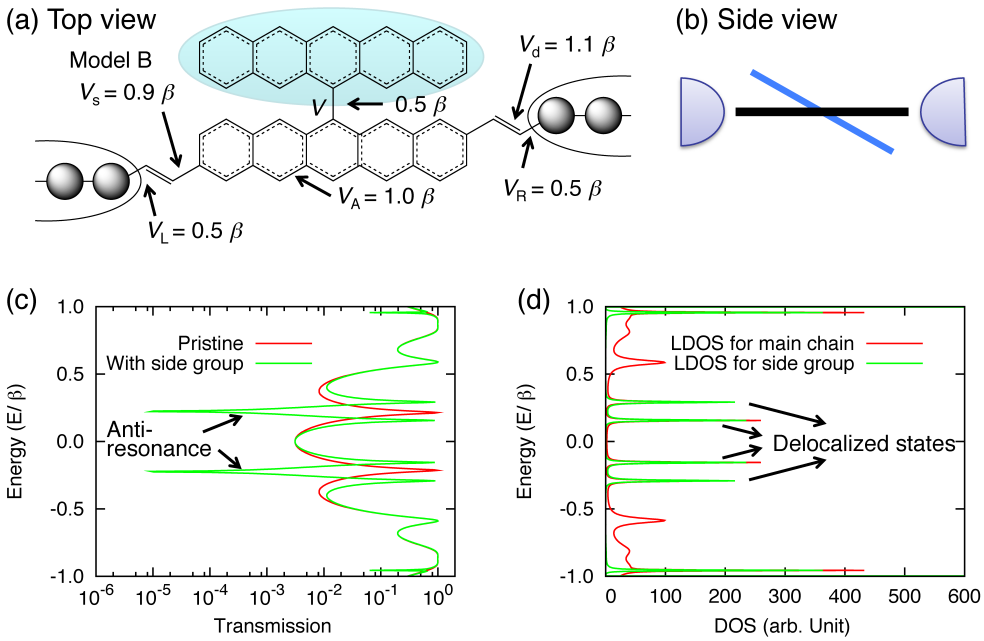

Figure 6: Demonstration of anti-resonance in a T-shaped molecular junction using the Hückel model: (a) Tight-binding scheme for a molecular junction (model B) with a side group using the Hückel model. Coupling between the molecule and left (right) 1D electrode is set to $V_{\mathrm{L/R}} = 0.5\beta$. The transfer integrals for aromatic carbons, single bond, and double bonds are set to $V_{\mathrm{A}} = 1.0\beta$, $V_{\mathrm{s}} = 0.9\beta$, and $V_{\mathrm{d}} = 1.1\beta$, respectively. The transfer integral V between the side chain and the main chain is reduced to 0.5β because of the torsion which could be caused by the steric repulsion as shown in panel (b). All transfer integrals are normalized in β. Transfer integrals in the electrodes are set to β. All on-site energies are set to 0. Side group is highlighted in light blue. (b) Side view of molecular junction. Because of the steric repulsion between the main chain and the side group, the side chain would be twisted. (c) Transmission spectra through the molecular device depicted schematically on panel (a) with pristine one. Since the eigen energies of the side fragment are almost identical with the ones of the main chain the resonant peaks of the main chain split into two resonance showing anti-resonances in the middle of resonant peaks. (d) local DOS plots for the side group and the main chain.

Acknowledgements

We gratefully acknowledge support from the German Excellence Initiative via the Cluster of Excellence EXC 1056 "Center for Advancing Electronics Dresden" (cfAED). We also gratefully acknowledge for funding by the European Union (ERDF) and the Free State of Saxony via TP A2 (MolFunc) of the cluster of excellence European Center for Emerging Materials and Processes Dresden (ECEMP), by the European Union (ERDF) and the Free State of Saxony via the ESF project 080942409 InnovaSens, and by World Class University program funded by the Ministry of Education, Science and Technology through the National Research Foundation of Korea (R31-10100).

References

[1] Miroshnichenko A E, Flach S and Kivshar Y S 2010 *Rev. Mod. Phys.* **82** 2257
[2] Kang K, Cho S Y, Kim J J and Shin S C 2001 *Phys. Rev. B* **63** 113304
[3] Ladrón de Guevara M L, Claro F and Orellana P A 2003 *Phys. Rev. B* **67** 195335
[4] Ratner M A 1990 *J. Phys. Chem.* **94** 4877
[5] D'Amato J L, Pastawski H M and Weisz J F 1989 *Phys. Rev. B* **39** 3544

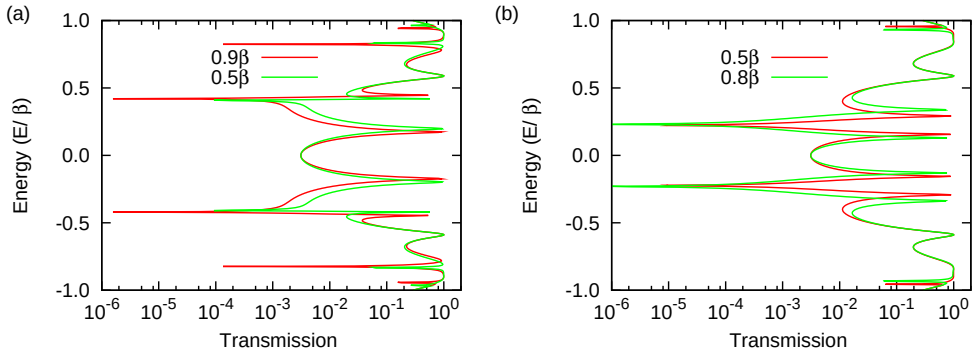

Figure 7: Dependence of line shape of transmission functions on the coupling strength between side groups and main chains in two model systems. (a) In model A, the reduction of the coupling V sharpens the Fano resonances. (b) In model B, the increase of the coupling strength V enhances the splitting of the two resonance peaks across the anti-resonance.

[6] Levstein P R, Pastawski H M and D'Amato J L 1990 *J. Phys.: Cond. Matt. 2* 1781
[7] Emberly E G and Kirczenow G 1999 *J. Phys.: Cond. Matt.* **11** 6911
[8] Papadopoulos T A, Grace I M and Lambert C J 2006 *Phys. Rev. B* **74** 193306
[9] Stafford C A, Cardamone D M and Mazumdar S 2007 *Nanotechnology* **18** 424014
[10] Solomon G C, Andrews D Q, Hansen T, Goldsmith R H, Wasielewski M R, Van Duyne R P and Ratner M A 2008 *J. Chem. Phys.* **129** 054701
[11] Solomon G C, Andrews D Q, Van Duyne R P and Ratner M A 2009 *ChemPhysChem* **10** 257
[12] Hansen T, Solomon G C, Andrews D Q and Ratner M A 2009 *J. Chem. Phys.* **131** 194704
[13] Guédon C M, Valkenier H, Markussen T, Thygesen K S, Hummelen J C and van der Molen S J 2012 *Nat. Nanotechnol.* **7** 305
[14] Tada T and Yoshizawa K 2002 *ChemPhysChem* **3** 1035
[15] Walczak K 2004 *Euro. J. Chem.* **2** 524
[16] Stadler R and Markussen T 2011 *J. Chem. Phys.* **135** 154109
[17] Nozaki D, Sevinçli H, Avdoshenko S M, Gutierrez R and Cuniberti G 2012 *Preprint* arXiv:1203.5269v3
[18] Fisher D S and Lee P A 1981 *Phys. Rev. B* **23** 6851
[19] Breit G and Wigner E 1936 *Phys. Rev.* **49** 519